Hindawi
Advances in Civil Engineering
Volume 2023, Article ID 9856964, 1 page
https://doi.org/10.1155/2023/9856964

Retraction

Retracted: Study on Seismic Performance of Recycled Steel Fibers Locally Reinforced Cruciform Concrete Frame Beam-Column Joint

Advances in Civil Engineering

Received 10 October 2023; Accepted 10 October 2023; Published 11 October 2023

This article has been retracted by Hindawi following an investigation undertaken by the publisher [1]. This investigation has uncovered evidence of one or more of the following indicators of systematic manipulation of the publication process:

(1) Discrepancies in scope
(2) Discrepancies in the description of the research reported
(3) Discrepancies between the availability of data and the research described
(4) Inappropriate citations
(5) Incoherent, meaningless and/or irrelevant content included in the article
(6) Peer-review manipulation

The presence of these indicators undermines our confidence in the integrity of the article's content and we cannot, therefore, vouch for its reliability. Please note that this notice is intended solely to alert readers that the content of this article is unreliable. We have not investigated whether authors were aware of or involved in the systematic manipulation of the publication process.

Wiley and Hindawi regrets that the usual quality checks did not identify these issues before publication and have since put additional measures in place to safeguard research integrity.

We wish to credit our own Research Integrity and Research Publishing teams and anonymous and named external researchers and research integrity experts for contributing to this investigation.

The corresponding author, as the representative of all authors, has been given the opportunity to register their agreement or disagreement to this retraction. We have kept a record of any response received.

References

[1] Y. Li, R. Zhao, D. Li, and C. Qu, "Study on Seismic Performance of Recycled Steel Fibers Locally Reinforced Cruciform Concrete Frame Beam-Column Joint," *Advances in Civil Engineering*, vol. 2022, Article ID 8155038, 19 pages, 2022.

Hindawi
Advances in Civil Engineering
Volume 2022, Article ID 8155038, 19 pages
https://doi.org/10.1155/2022/8155038

Research Article

Study on Seismic Performance of Recycled Steel Fibers Locally Reinforced Cruciform Concrete Frame Beam-Column Joint

Yan Li, Rong-Hua Zhao, Dong-Yi Li, and Chang Qu

School of Civil Engineering, Jilin Jianzhu University, Changchun, Jilin Province, China

Correspondence should be addressed to Dong-Yi Li; lidongyi@student.jlju.edu.cn

Received 16 December 2021; Revised 7 January 2022; Accepted 30 January 2022; Published 25 March 2022

Academic Editor: Ramadhansyah Putra Jaya

At present, concrete frame structures are widely used, and the frame beam-column joints are the key parts of the whole frame in seismic resistance. In previous studies, recycled steel fiber-reinforced concrete is a new type of environment-friendly reinforcement material, which can also be widely used in the construction industry. Therefore, in this paper, MTS electrohydraulic servo loading systems were used to carry out low-cycle reciprocating cyclic loading tests to study the seismic performance of five 1/2 scale cruciform concrete frame beam-column joint specimens with plain concrete, normal steel fiber-reinforced concrete, and three recycled steel fiber-reinforced concrete with different fiber contents in the joint core area. The results show that the addition of normal steel fibers can improve the bearing capacity, ductility, energy dissipation capacity, and shear strength of concrete frame joint specimens and delay the stiffness degradation of joint specimens, recycled steel fibers can improve the seismic performance of the cruciform concrete frame joints better than normal steel fibers, and the seismic performance increases gradually with the increases of volume ratio of recycled steel fibers. Moreover, with the recycled steel fiber content from 0.5% to 1.0% and then to 1.5%, the increased amplitude of the seismic performance of joint specimens increases. Considering the reinforcing effect of recycled steel fibers on concrete matrix and based on the design formula of shear capacity of reinforced concrete joints, the design formulas of shear capacity of recycled steel fiber-reinforced concrete beam-column joints were established by using the statistical analysis method and the baroclinic rod-truss model, and the calculation results were in good agreement with the test results. This study can provide references for seismic performance research of steel fiber-reinforced beam-column joints and the recycling of steel wire from waste tires.

1. Introduction

Reinforced concrete frame structure has been widely used in various fields of construction industry because of its good seismic performance. It is found that, under earthquake load, the frame beam-column joints are subjected to complex stress and are prone to brittle shear failure [1]. Adding normal steel fibers into the frame joint core area can improve the bonding strength between longitudinal bars and concrete and enhance the ductility and energy dissipation capacity of frame joints [2, 3]. The industrial recycled steel fibers formed by cutting high-quality steel wire extracted from waste tires also have higher hardness, breaking force, elongation, torsion strength, tensile strength, and yield strength [4]. It can be mixed into concrete according to a certain volume ratio to prepare a new hybrid high-performance environmental protection composite material, which will have a good application prospect in construction industry. In foreign countries, the steel wire from waste tires has been made into high-performance wire mesh, spring, and so on for housing construction, water conservancy, and other construction projects. And although the price of industrial recycled steel fibers is similar to or slightly higher than that of normal steel fibers and because the volume of normal steel fibers is small, the amount of normal steel fibers under the same volume rate is much more than that of recycled steel fibers, so the use of recycled steel fibers in engineering is more economic and reasonable than normal steel fibers. And according to statistics, in recent years, the production of waste tires in China and the world has been huge [5]; the wire accounts for 15~20% of the total weight of a waste tire. Therefore, making recycled steel fibers from waste tires as a reinforcement

material can not only save resources and protect the environment but also provide a new research direction for the improvement of the harmless utilization rate of waste tires and the green and sustainable development of the country [6, 7].

2. Research Background

Kheni et al. [8] studied the ductility of fiber-reinforced concrete beam-column joints, and the results showed that adding hybrid fibers into the joint part of the specimen could effectively improve the displacement ductility and energy dissipation capacity of the specimen. Liang et al. [9] studied the seismic performance of fiber-reinforced concrete interior beam-column joints, and the results showed that steel fibers can effectively improve the seismic performance of concrete beam-column joints. Shang. [10] conducted an experimental study on the seismic performance of steel fibers locally reinforced high-strength concrete frame joints, and the results show that steel fibers can improve the shear strength of frame joints, and with the increases of the volume ratio of steel fibers in the frame joints, the ductility and energy dissipation capacity of specimens are significantly improved, and the degradation of bearing capacity and stiffness is delayed.

However, the research mainly focused on the performance of normal steel fiber-reinforced frame beam-column joints, and the research on the performance of recycled steel fiber-reinforced frame joints is also less, so in this paper, five cruciform reinforced concrete frame beam-column joint specimens were designed, and three of the specimens were mixed with recycled steel fibers of different volume rate in their joints. The low-cycle reciprocating cyclic loading test was carried out on the specimens, and the seismic performance of beam-column joints was theoretically analyzed and experimentally studied. Under the condition of considering the reinforcing effect of recycled steel fibers on concrete matrix, a calculation model of shear capacity of recycled steel fiber-reinforced concrete frame joints was established by using the design formula of shear capacity of reinforced concrete joints. This study can provide references for the engineering application of concrete beam-column joints and the recycling of steel wire from waste tires.

3. Experimental Programs

3.1. Experimental Materials. In this test, copper-coated microwire steel fibers were selected as normal steel fibers, bending 100% without fracture and tensile strength more than 2850 MPa. The recycled steel wire was selected from straight round steel wire from waste tires of a company, which was manually polished and cut. To ensure the effective bonding length between recycled steel fibers and concrete [11], many experts and scholars have conducted in-depth studies and found that recycled steel fibers with a length-diameter ratio above 30 can play the bridging role with concrete better. Therefore, recycled steel fibers with a length-diameter ratio above 40 were adopted in this experiment. The basic characteristic parameters of recycled steel fibers are shown in Table 1 and the sheared recycled steel fibers are shown in Figure 1. The longitudinal bars of the beams and columns are HPB300 grade rebars, and the stirrups are HRB400 grade rebars. Concrete material properties of the five specimens are shown in Table 2.

3.2. Design of Specimens. In order to simplify the test, the cruciform concrete frame beam-column joint was selected for the specimen as shown in Figure 2 [12], and the reinforcement of the specimen is shown in Figure 3, with only horizontal or vertical force at the boundary. According to relevant regulations, the size of the frame joint specimen in the quasistatic loading test should be greater than or equal to 1/4 of the prototype [13], so the specimen adopted a 1/2 scale according to the actual situation of the laboratory. The beam in the specimen is 3.1 m long, the section size is 250×400 mm, the column height is 2.8 m, and the section size is 300×300 mm. The axial compression ratio was selected as 0.2. Among the five specimens, specimen SJ-1 is an ordinary reinforced concrete specimen. According to various theories of fiber reinforcement mechanism, such as fiber spacing theory and composite material theory [14, 15], fiber volume ratio is one of the main factors affecting the fiber reinforcement effect. According to relevant research data on the flexural performance of recycled steel fibers, adding 0.5%~1.5% industrial recycled steel fibers into concrete can effectively improve the mechanical properties of concrete [16]. Therefore, specimens SJ-2, SJ-3, and SJ-4 are recycled steel fiber-reinforced concrete specimens with a fiber volume ratio of 0.5%, 1.0%, and 1.5%, respectively. Specimen SJ-5 is a reinforced concrete specimen mixed with 0.5% normal steel fibers. The steel fibers were uniformly distributed in the concrete beam-column joints, and the mixing position of recycled steel fibers and normal steel fibers was 1.5 times the height of the beam from the column edge [17].

3.3. Loading System and Measurement Content and Method. During the earthquake, the damage of the general high-rise building is mainly caused by horizontal vibration, while the damage of the concrete frame beam-column joints in the low-rise building is generally caused by the vertical load. Therefore, the vertical low-cycle reciprocating cyclic loading test is adopted in this test to simulate the earthquake load. In the test, the large reaction walls, a reaction beam, and a 100 T hydraulic Jack were used to apply 500 kN vertical axial pressure on the top of the column, and the top and bottom of the column are fixed by hinge supports. Two symmetric MTS electrohydraulic servo loading systems with stroke of ±250 mm and maximum range load of 650 kN were used to carry out a low-cycle reciprocating cyclic loading test on the beam end of the specimen, as shown in Figure 4.

Displacement loading method was used in the test. Before the test, the axial force of an axial compression ratio of 0.2 was gradually applied on the top of the specimen column. At this time, the MTS actuator retained a certain distance from the beam end to ensure that the beam end was free and no internal force was generated before the test began. The vertical force remained constant during the test.

Table 1: Material performance parameters of recycled steel fibers.

Type	Average length (mm)	Effective diameter (mm)	Fusibility (C)	Specific gravity (kg m^2)	Tensile strength (MPa)
Round straight	60	1.5	258	40	1800

Figure 1: Recycled steel fibers.

Table 2: Material properties of concrete.

No.	The compressive strength of a prism (MPa)	Axial compressive strength (MPa)	Elasticity modulus (MPa)
SJ-1	40.34	35.07	3.27×10^5
SJ-2	45.25	42.15	3.29×10^5
SJ-3	47.53	43.23	3.29×10^5
SJ-4	50.14	45.37	3.31×10^5
SJ-5	44.05	40.55	3.28×10^5

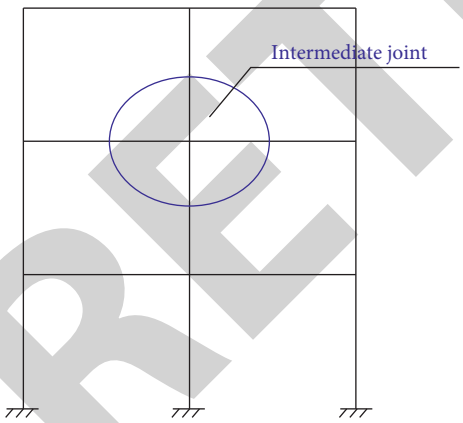

Figure 2: Captured schematic diagram of the frame joint.

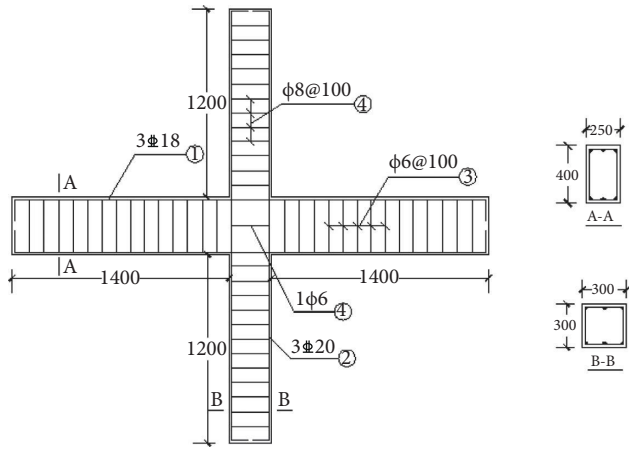

Figure 3: Reinforcement diagram of the specimen.

Then, the displacement-controlled loading was carried out according to the loading method in Figure 5. In the process of testing, one MTS actuator applied an upward force, while the other applied a downward force, then returned to zero at the same time, then acted in the opposite direction, and finally returned to zero at the same time, thus forming a low-cycle reciprocating loading. The pre-pasted resistance strain gauge was used to connect the IMP acquisition plate to measure the strain of beam-column joint core areas, the beam longitudinal reinforcements, the column longitudinal reinforcements, and the column stirrups. The layout of longitudinal strain gauges is shown in Figure 6, and the layout of stirrup strain gauges is shown in Figure 7. The column end displacement and angle of beam end plastic hinge area near the joint were measured by the displacement meter arranged in Figure 8. The development of cracks was observed visually, and the crack width was measured by the ZBL-F103 Fazhibolian crack width meter independently developed by Beijing.

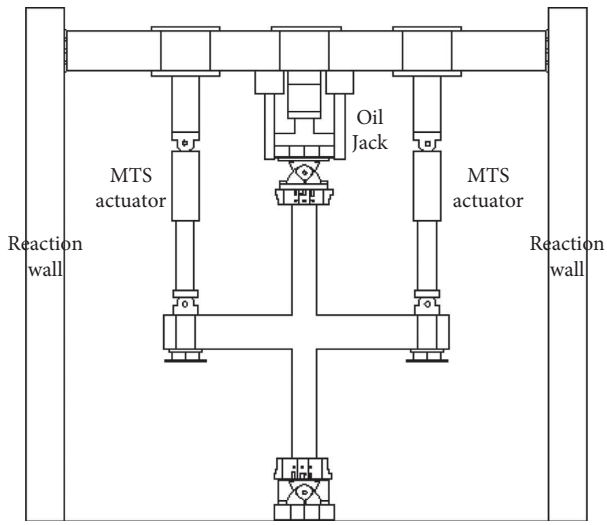

Figure 4: Schematic diagram of test equipment and loading.

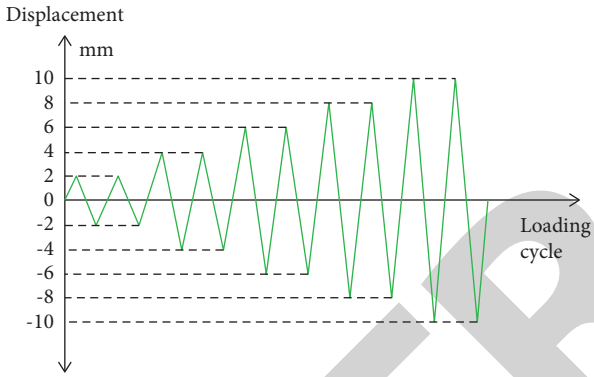

Figure 5: The loading system of specimens.

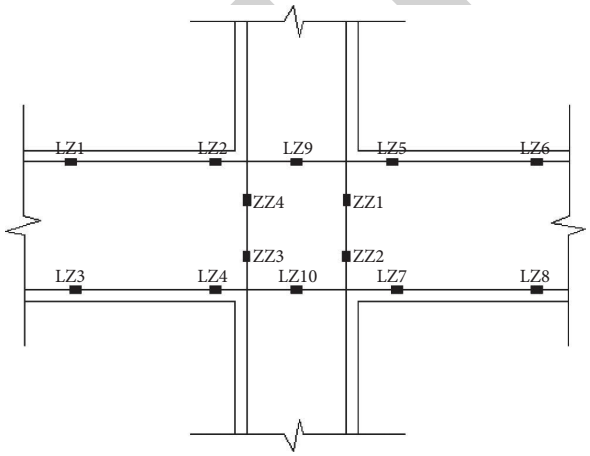

Figure 6: Layout of longitudinal reinforcement strain gauges.

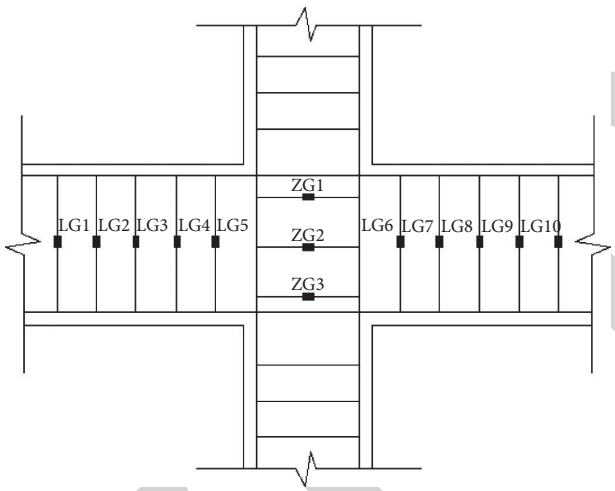

Figure 7: Layout of stirrup strain gauges.

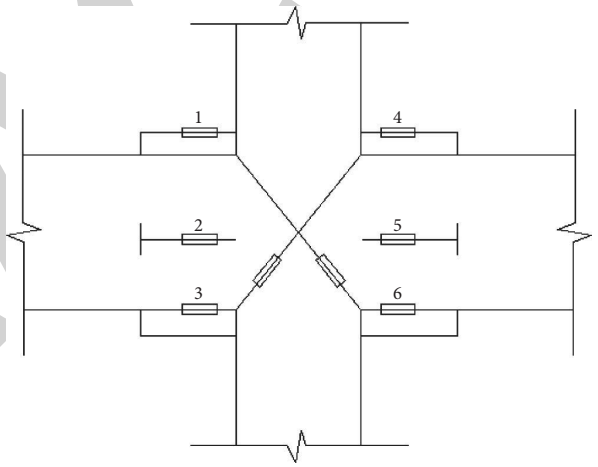

Figure 8: Layout of displacement meter.

4. Failure Phenomenon and Result Analysis of Specimens

4.1. Failure Phenomenon of Specimens. Specimen SJ-1 was ordinary reinforced concrete. When the displacement cycle reached +10 mm, the first inclined crack appeared in the joint area, with a width of 0.01 mm and a length of 37 cm, and several tiny cracks appeared near the beam end of the joint area. When the displacement cycle reached −16 mm, an inverted inclined crack with a width of 0.01 mm and a length of 35 cm appeared in the joint area. When the cycle reached +22 mm, the peak load reached 97.68 kN, and a tiny crack parallel to the main inclined crack appeared in the joint area. When the displacement cycle reached +24 mm, the specimen had a clicking sound, the main inclined crack deepened, and the crack widened to 0.42 mm. When +28 mm, the two main cracks in the core area along the diagonal direction widened to 1.36 mm, and the width of tiny cracks increased obviously. A small area of concrete spalled on the surface of the joint area at −32 mm. When the displacement cycle reached −34 mm, the bearing capacity of the specimen decreased to below 80%. The final failure mode of specimen SJ-1 is shown in Figure 9(a).

Specimen SJ-4 is a reinforced concrete specimen mixed with 1.5% recycled steel fibers. When the displacement cycle reached +18 mm, the first main inclined crack with a width of 0.01 mm and a length of 15 cm appeared in the joint area,

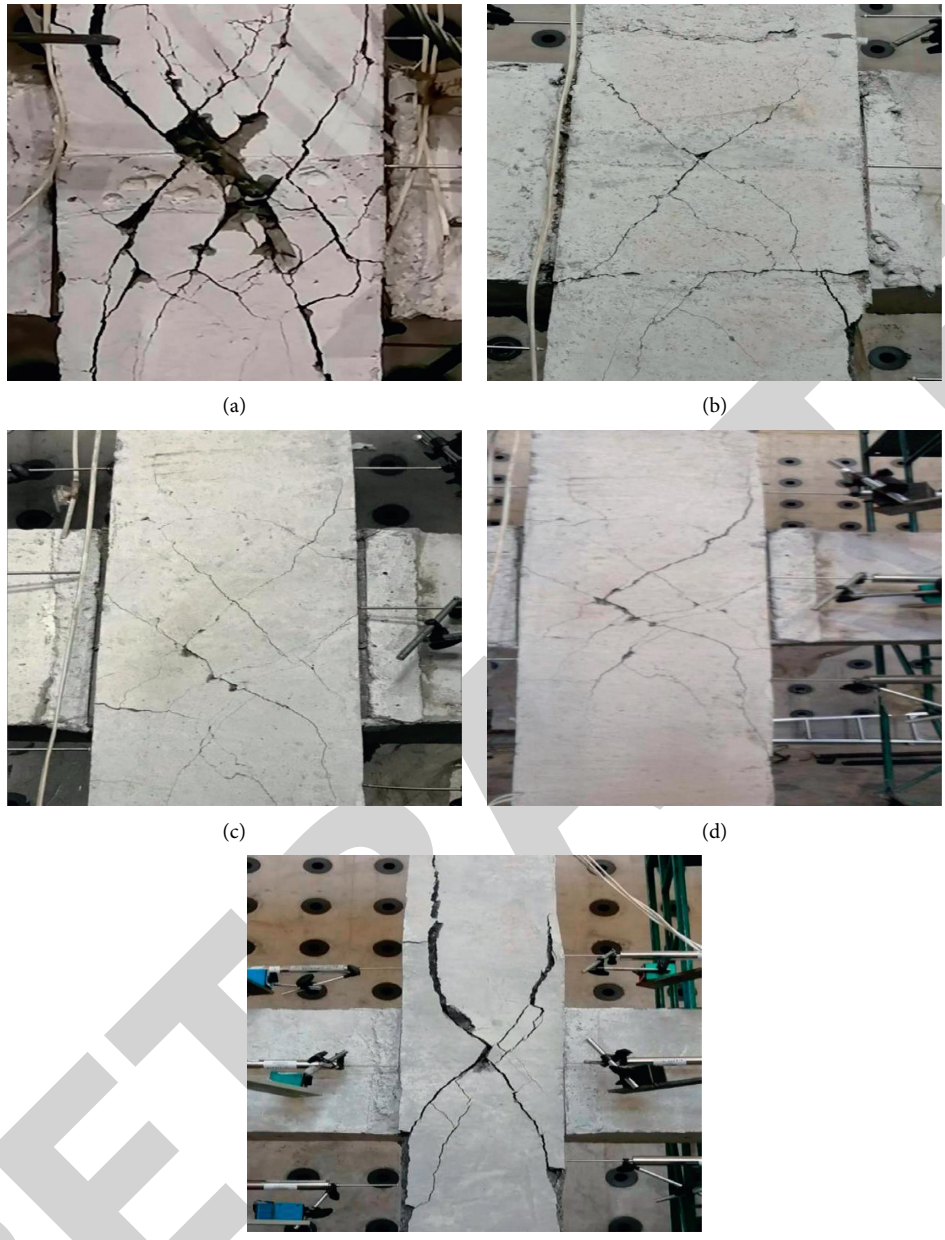

(a) (b) (c) (d) (e)

Figure 9: Final failure mode of specimens. (a) SJ-1. (b) SJ-2. (c) SJ-3. (d) SJ-4. (e) SJ-5.

and a horizontal crack with a length of 15 cm appeared in the lower side of the column. An oblique tiny crack appeared in the beam end near the left side of the joint area, 30 cm away from the beam end. At +24 mm, "X-shaped" cracks appeared in the joint area, accompanied by tiny cracks parallel to the main cracks. When the displacement cycle reached +28 mm, the ultimate load of the specimen reached 100.87 kN, the main crack in the joint area widened to 0.67 mm, and the horizontal cracks at the column end formed a small through-crack. At +32 mm, two small tiny cracks appeared near the column end of the joint area, and the soil mass on the concrete surface fell off. At +38 mm, the tiny cracks in the joint area increased, the tiny cracks near the joint area lengthened, and the crack width reached 1.65 mm. When the displacement circulated to −44 mm, there was a large area of soil spalled near the column end of the joint core area. The final failure mode of specimen SJ-4 is shown in Figure 9(d).

Specimen SJ-5 was a reinforced concrete specimen mixed with 0.5% normal steel fibers. When the displacement cycle reached +12 mm, inclined cracks appeared in the plastic hinge area on the left side of the joint 40 cm from the beam end, with a length of 35 cm. At +16 mm, another crack appeared in the opposite direction to the main crack, forming a cross crack with it, and short fine cracks appeared on both sides of the column end at the joint. When the displacement cycle reached −20 mm, the tiny crack perpendicular to the oblique crack was extended to 28 cm, and other small cracks were still extended continuously. At

−22 mm, the peak load of the specimen reached 98.31 kN, a tiny crack with a length of 30 cm parallel to the second main crack appeared in the joint area, and the number of tiny cracks in the joint area increased. When the displacement cycle reached −38 mm, the main crack in the joint area extended to the column end, and the width of the crack increased to 1.45 mm. A small area of soil spalled occurred in the joint area, and many tiny cracks perpendicular to the main crack appeared. When the bearing capacity of the specimen decreased to below 80% of the peak load, the test stopped. The final failure mode of specimen SJ-5 is shown in Figure 9(e).

The macroscopic test phenomenon of specimens SJ-2 and SJ-3 is basically similar to that of specimen SJ-4. The failure modes of joints are different due to the different volume ratios of recycled steel fibers. Compared with SJ-4, the number of cracks in the joint core area of specimens SJ-2 and SJ-3 increased significantly, and their widths increased significantly when specimens SJ-2 and SJ-3 were destroyed. The situation of cracks development and failure of specimen SJ-3 are better than that of specimen SJ-2. See Figure 9(b) and Figure 9(c) for their final failure patterns. Referring to relevant literature and test results [18], the failure modes of five joint specimens can be obtained as shown in Table 3.

4.2. Result Analysis

4.2.1. Hysteretic Curves Analysis of Specimens. Under the quasistatic action, load-displacement curves of steel fiber-reinforced concrete beam-column joint specimens with different fiber types and fiber volume contents and ordinary reinforced concrete beam-column joint specimens are shown in Figure 10.

According to Figure 10, the hysteretic curves of five joint specimens are all close to S shape. In the early stage of the test displacement cycles, the specimens were in the elastic working stage, and the load-displacement curves changed linearly. The hysteretic curves were approximately a straight line, almost no residual deformation occurred, and stiffness degradation was not obvious. However, as the number of displacement cycles increased, cracks began to appear in the specimen. At this time, the load-displacement curves began to show nonlinear changes, the hysteretic curves were no longer linear, and their area was also increasing. The specimens began to show large residual deformation, and stiffness degradation became obvious. As the specimens reached the ultimate loads and then the failure loads, the fullness of the hysteretic curve of specimen SJ-1 was worse than that of the other four specimens, the number of displacement cycles was relatively less, and stiffness degradation was obvious. For specimens SJ-2~SJ-4, the cracking loads, yield loads, ultimate loads, and their corresponding displacement of specimens all gradually increase with the increases of recycled steel fiber content. Moreover, when the recycled steel fiber content increases from 0.5% to 1.0% and then to 1.5%, the increased amplitude of the three kinds of load and their corresponding displacement of joint specimens all becomes larger. However, the ultimate load of specimen SJ-2 was slightly smaller than that of specimens SJ-1 and SJ-5, which may be caused by nonuniform mixing during pouring concrete or uneven watering during curing. It can also be seen from the hysteretic curves of all specimens that the overall slope of the hysteretic curve of specimen SJ-1 is the smallest; that is, the stiffness of specimen SJ-1 is the smallest. However, from specimen SJ-5 to SJ-2 to SJ-4, the slope of the hysteretic curves is gradually increased; that is, the stiffness of the specimens is gradually increased. In addition, it can be seen that the stiffness of the four specimens gradually degrades, and compared with specimen SJ-1, the capacity of dissipation earthquake and deformation of specimens SJ-2~SJ-4 is gradually improved; that is, the ductility of specimens is gradually improved.

(1) Under the action of low-cycle reciprocating cyclic loading, the cross-cracks appeared in the joint core area of specimen SJ-1 for a very short time, there were many cracks in the joint core area, and the crack width was the largest. The joint core areas of specimens SJ-2~SJ-5 have good toughness and multiple cracking properties under load. The initial cracking of the joint surface was later than that of SJ-1, and the joint core area mixed with recycled steel fibers showed a large number of tiny cracks, indicating that the crack resistance of specimens has been improved to a certain extent.

(2) From the hysteresis curves of specimens SJ-2 to SJ-4 (Figures 10(b)–10(d)), it can be seen that the ultimate bearing capacity of three specimens increases gradually, but there is little difference. The stiffness degradation of specimen SJ-4 was slower than that of SJ-2 and SJ-3. Therefore, the increase of recycled steel fiber content does not significantly improve the bearing capacity of specimens [19] but has a relatively obvious improvement in the ductility and the delay of stiffness degradation of specimens [20].

(3) Specimen SJ-2 and specimen SJ-5 are used as comparison specimens; it can be seen that the bearing capacity and stiffness degradation capacity of specimen SJ-2 are slightly stronger than that of specimen SJ-5, and specimen SJ-2 has fewer cracks than specimen SJ-5, indicating that recycled steel fibers can improve the seismic performance of joint specimens better than normal steel fibers.

4.2.2. Skeleton Curves Analysis of Specimens. As can be seen from the comparison diagrams of skeleton curves of specimens in Figure 11, the ultimate loads and ultimate displacements of the joint specimens mixed with steel fibers in the joint core area are increased to varying degrees. Before yielding, the specimens were in the elastic stage, and the skeleton curves were approximately a straight line. When the inflection point of the skeleton curve of specimen SJ-1 appeared, the curves of specimens SJ-2~SJ-5 continued to rise with the increase of the displacements. The time of inflection point of the curve of specimen SJ-4 is the latest, and the ultimate load value is the largest. Comparing specimen SJ-2 and SJ-5, specimen SJ-2 showed better

Table 3: Test results.

No.	Cracking load (kN)	Cracking displacement (mm)	Yield load (kN)	Yield displacement (mm)	Ultimate load (kN)	Ultimate displacement (mm)	Failure mode
SJ-1	78.14	10	84.75	16.18	97.68	21.94	Shear and bending failure
SJ-2	79.78	13	85.59	17.82	96.71	25.59	Shear and bending failure
SJ-3	81.26	15	88.24	18.31	98.67	25.73	Shear failure
SJ-4	84.49	18	95.68	19.23	100.87	25.95	Shear failure
SJ-5	79.21	12	85.31	16.68	98.31	22.21	Shear and bending failure

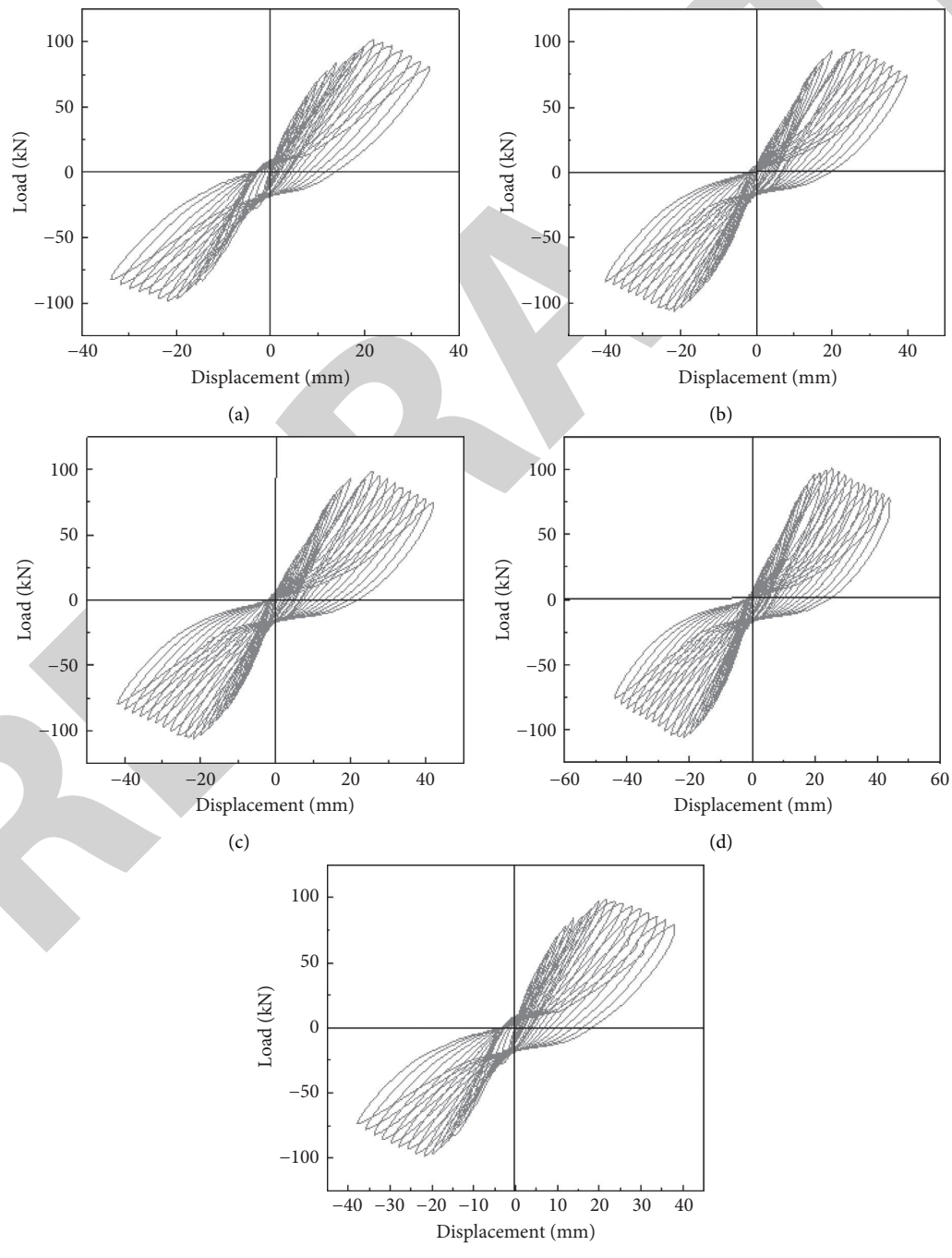

Figure 10: Hysteretic curves of specimens. (a) SJ-1. (b) SJ-2. (c) SJ-3. (d) SJ-4. (e) SJ-5.

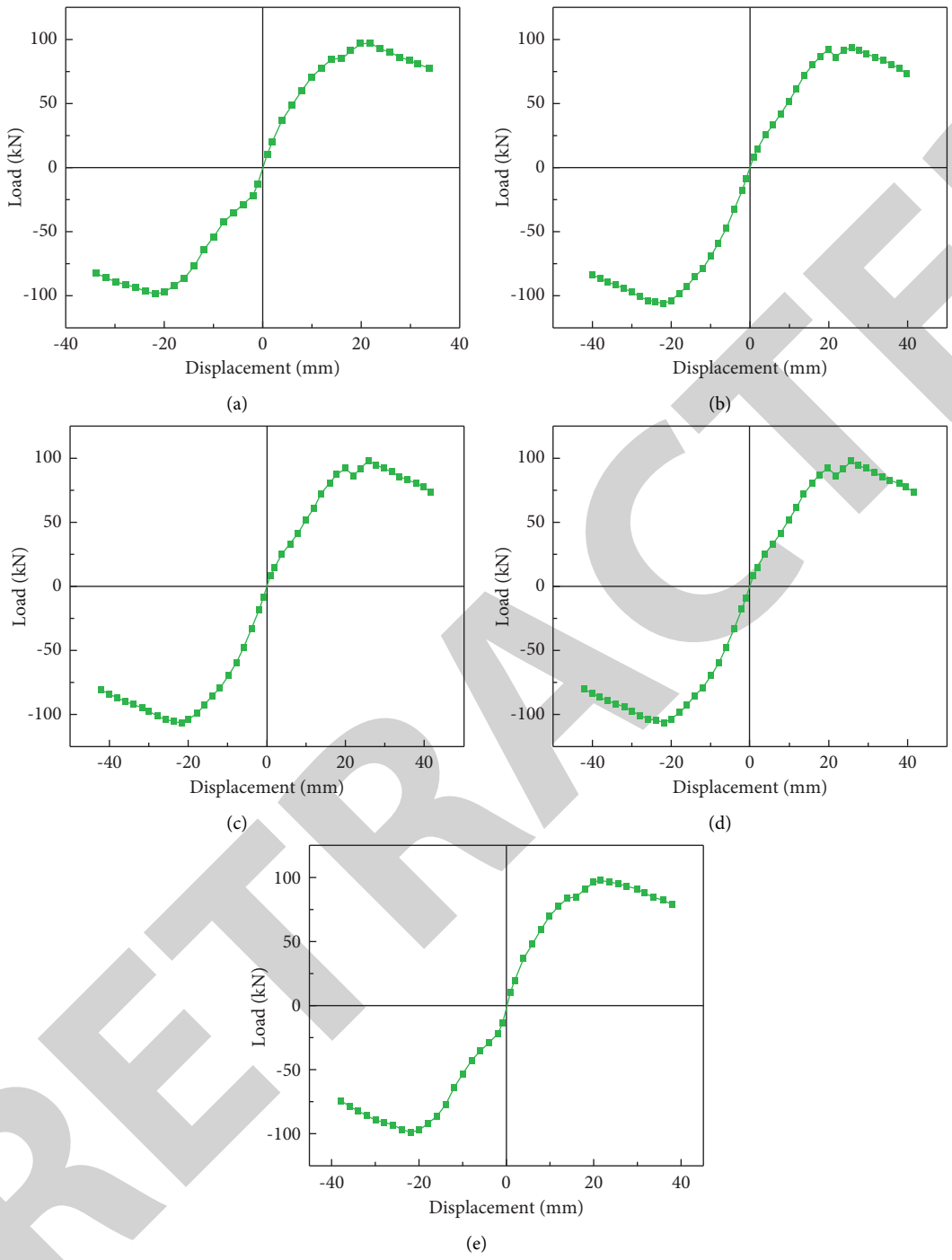

Figure 11: Skeleton curves of specimens. (a) SJ-1. (b) SJ-2. (c) SJ-3. (d) SJ-4. (e) SJ-5.

strength. Based on the skeleton curve analysis, it can be concluded that the seismic bearing capacity of specimens can be improved by adding steel fibers in the joint area, and except the ultimate load of specimen SJ-2, the cracking loads, yield loads, ultimate loads, and their corresponding displacements of the joint specimens mixed with recycled steel fibers in the joint core area are increased to a greater extent; that is, the effect of recycled steel fibers on strengthening the crack resistance of specimens is better than that of normal steel fibers.

4.2.3. Ductility Analysis of Specimens. The ductility discussed in this paper is the deformation capacity that the bearing capacity remains in a relatively stable state after the beam end section near the joint area rises from the yield to the maximum bearing capacity. The good ductility of the specimen can show that it still has the ability to consume earthquake after yielding or reaching the ultimate bearing capacity and can avoid the occurrence of brittle failure of the specimen.

In this paper, the characteristic values of bearing capacity and displacement ductility of specimens were obtained by the "energy equivalence method," the principle of which is shown in Figure 12. The yield load P_y and yield displacement Δ_y of specimens were determined according to the skeleton curve of each specimen, the failure load was set as $P_u = 0.8P_{max}$, and the failure displacement Δ_u was the corresponding displacement value of the failure load. The ductility of specimens is calculated according to the ratio of failure displacement to yield displacement of specimens, as shown in formula (1). The characteristic values of bearing capacity and ductility coefficient of specimens are shown in Table 4.

$$\mu = \frac{\Delta_u}{\Delta_y}, \tag{1}$$

where μ is the displacement ductility coefficient; Δ_u is the failure displacement (mm); Δ_y is the yield displacement (mm).

It can be seen from the table that the addition of normal steel fibers can improve the ductility of specimens, the recycled steel fibers can improve the ductility of specimens better than normal steel fibers, and the ductility of specimens gradually improves with the increase of the volume ratios of recycled steel fibers. Moreover, with the recycled steel fiber content from 0.5% to 1.0% and then to 1.5%, the increased amplitude of the ductility performance of joint specimens increases.

4.2.4. Stiffness Degradation Analysis of Specimens. The stiffness degradation is mainly caused by the bonding degradation between rebars and concrete after the cracking of beam-column joints and the cumulative development of some tiny cracks in the macroscopic expression of specimen damage. Stiffness degradation can reflect the fatigue damage and the whole process from the beginning of loading to yield to failure of the specimen under cyclic loading [21].

The index used in this paper to evaluate stiffness degradation of specimens under low-cycle reciprocating cyclic loading is secant stiffness. The specimens in the test in this paper are evaluated and analyzed according to secant stiffness. The design formula is as follows:

$$K_i = \frac{\left|V_i^+\right| + \left|V_i^-\right|}{\left|\Delta_i^+\right| + \left|\Delta_i^-\right|}, \tag{2}$$

where K_i is the secant stiffness in the i cycle; V_i^+ and V_i^- are the ultimate load of the specimen in the i cycle; Δ_i^+ and Δ_i^- are the displacement value corresponding to the peak load in the i cycle.

According to the comparative analysis of stiffness curves of all specimens in Figure 13, it can be seen that, compared with the reinforced concrete specimens mixed with recycled steel fibers in the joint core area, the initial stiffness of both the ordinary reinforced concrete specimen and the concrete specimen mixed with normal steel fibers is slightly higher. However, the slope of the curve is also very high, which is mainly affected by the early shear failure at the joint. The ductility of the joint is greatly enhanced by the addition of recycled steel fibers, so the slope of the curves of specimens

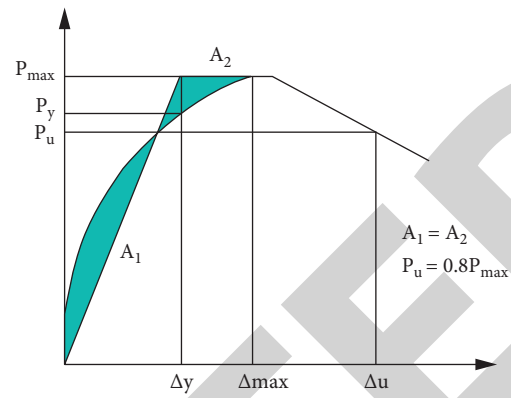

Figure 12: Principle of energy equivalence method.

SJ-2~SJ-4 is much lower, and with the recycled steel fiber content from 0.5% to 1.0% and then to 1.5%, the amplitude of the stiffness degradation of joint specimens decreases. After the inflection point of the curves, the decreasing rate of stiffness degradation curves of all specimens slows down and tends to a gentle state.

4.2.5. Energy Dissipation Capacity Analysis of Specimens. Under the action of earthquake, the structure has the ability to absorb and dissipate seismic energy, and the calculation of the fixed value of the energy dissipation capacity of the specimen should be realized by using the equivalent viscous damping coefficient and power ratio index [22], and the larger the value is, the stronger the energy dissipation capacity of the structure is. In this paper, the energy dissipation performance of the structure is evaluated in general by calculating the energy dissipation coefficient and equivalent viscous damping coefficient.

In general, the dissipated energy of a structure usually refers to the area enclosed by the closed curve formed by the hysteretic curve. As shown in Figure 14, the structure energy dissipation coefficient (formula (3)) and equivalent viscous damping coefficient (formula (4)) are obtained by calculating the area of the hysteretic curve. See Table 5 for the results.

$$E = \frac{S_{(ABD+CDB)}}{S_{(OCE+OAF)}}, \tag{3}$$

where E is the structural energy dissipation coefficient; $S_{(ABD+CDB)}$ is the area enclosed by the hysteretic curve closed curve; $S_{(OCE+OAF)}$ is the area of triangle OCE and triangle OAF.

$$h_e = \frac{1}{2\pi} \cdot \frac{S_{(ABD+CDB)}}{S_{(OCE+OAF)}}, \tag{4}$$

where h_e is the equivalent viscous damping coefficient.

As can be seen from Table 5, the energy dissipation coefficient and equivalent viscous damping coefficient of specimens mixed with steel fibers in the joint core area are higher than the ordinary reinforced concrete specimen; especially, the specimen with recycled steel fibers content of 1.5% has the largest value. Compared with specimen SJ-2

Table 4: Characteristic values of bearing capacity and ductility coefficients of specimens.

No.	Yield point		Limit point		Breaking point		Displacement ductility
	P_y/kN	Δ_y/mm	P_{max}/kN	Δ_{max}/mm	P_u/kN	Δ_u/mm	μ
SJ-1	84.75	16.18	97.68	21.94	76.78	33.87	2.09
SJ-2	85.59	17.82	96.71	25.59	76.95	40.24	2.26
SJ-3	88.24	18.31	98.67	25.73	77.41	42.23	2.31
SJ-4	95.68	19.23	100.87	25.95	78.58	46.11	2.40
SJ-5	85.31	16.68	98.31	22.21	76.97	36.13	2.17

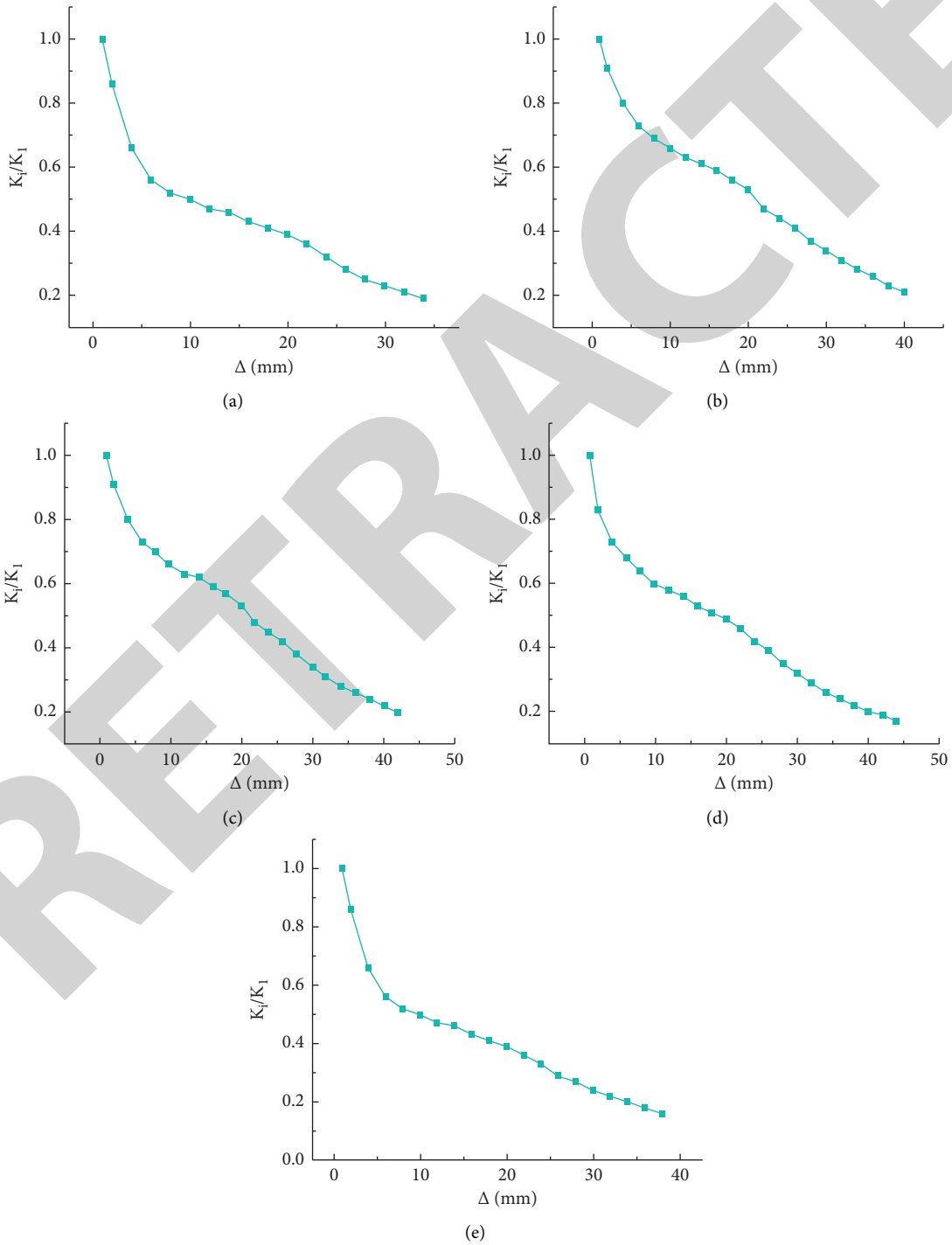

Figure 13: Stiffness degradation curves of specimens. (a) SJ-1. (b) SJ-2. (c) SJ-3. (d) SJ-4. (e) SJ-5.

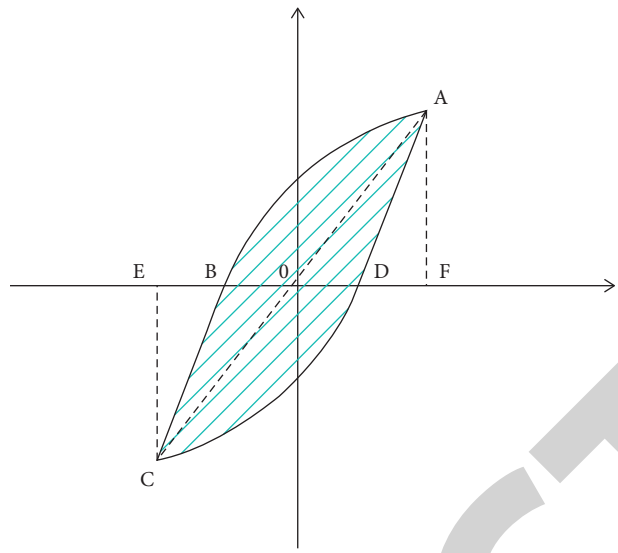

Figure 14: The area of the hysteretic curve.

Table 5: Equivalent viscous damping coefficient and energy dissipation coefficient of specimens at structural yield.

No.	Area enclosed by the hysteretic curve	Energy dissipation coefficient	Equivalent viscous damping coefficient (%)
SJ-1	528.91	0.41	6.53
SJ-2	541.75	0.47	7.48
SJ-3	576.48	0.54	8.59
SJ-4	663.83	0.66	10.50
SJ-5	533.84	0.43	6.84

and SJ-5 under the same content, specimen SJ-2 has a better effect than specimen SJ-5. According to the energy dissipation coefficient, equivalent viscous damping coefficient, and the above analysis, the energy dissipation capacity of specimens with steel fibers mixed in the joints and plastic hinge areas at both ends is greatly improved compared with the ordinary concrete specimen, the effect of recycled steel fibers on enhancing energy dissipation capacity is stronger than normal steel fibers, and the energy dissipation capacity of specimens increases with the increase of volume ratios of recycled steel fibers. Moreover, with the recycled steel fiber content from 0.5% to 1.0% and then to 1.5%, the increased amplitude of the energy dissipation capacity of joint specimens increases.

4.2.6. Shear Deformation Analysis of Specimen Joints. Under the action of quasistatic loading, there are two diagonal angles at the specimen joint area. Under the influence of the bidirectional pressure transmitted by the beam end and the column end and the tension transmitted by the bonding stress of the rebars, a group of cross diagonal tension pressures are formed at the joint. Under the joint influence of the two forces, the shear deformation in the joint core area is shown in Figure 15, resulting in the decline of the overall stability of the structure. The shear angle of the joint core area can be calculated by geometric analysis, as shown in Figure 15.

The shear deformation angle formula (5) is obtained from the geometric relationship in Figure 15:

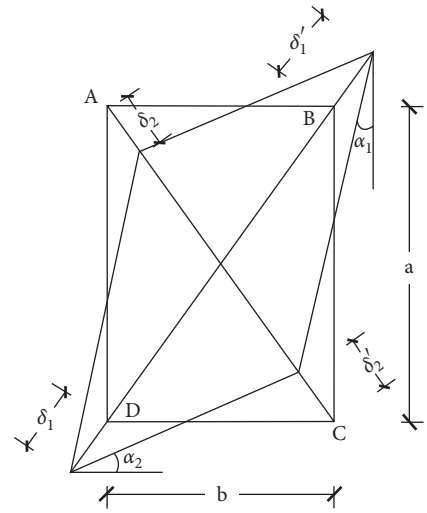

Figure 15: Geometric relation diagram of shear deformation in joint core area.

$$\gamma = \alpha_1 + \alpha_2 = \frac{\sqrt{a^2 + b^2}}{2ab}\left[\left(\delta_1 + \delta_1'\right) - \left(\delta_2 + \delta_2'\right)\right], \tag{5}$$

where γ is the sum of shear deformation angles in joint core area; α_1 and α_2 are the deformation angles of the two diagonal directions at the joint; a and b are the joint area dimensions (height and width); δ_1, δ_1', δ_2, and δ_2' are the

change values of the diagonals in the joint core area (stretching and compression).

The shear deformation angle value of each specimen under the first yield state and limit state is shown in Figures 16 and 17.

For specimens SJ-2~SJ-5, both the deformation angle under the first yield state and the deformation angle under the first limit state decrease compared with specimen SJ-1. In other words, under the condition of the same stirrup ratio, the concrete constraint ability in the joint core area was significantly improved after the recycled steel fibers were added, and the development of concrete inclined cracks in the joint core area was alleviated. As the shear deformation angle of specimen SJ-4 is 0.5 times that of specimen SJ-1, it can be seen that the recycled steel fibers with a high volume ratio have better crack resistance in the joint core area and can improve the overall stability of the structure. That is to say, with the increases of the volume ratio of recycled steel fibers, the shear angles of the specimen joint decrease gradually, and the stiffness and shear strength increase.

The beam end deflection δ_j caused by shear deformation at the joint is

$$\delta_j = l \cdot \gamma, \tag{6}$$

where l is the distance between the free end of the beam and the end of the joint and is taken as $l = 1500$ mm.

The calculated deflection value δ_j of the beam end is shown in Table 6.

5. Derivation of Design Formulas of Shear Capacity of Recycled Steel Fiber-Reinforced Cruciform Concrete Frame Joints

5.1. Action Mechanism of Shear Capacity of Recycled Steel Fiber-Reinforced Concrete Frame Joints. Frame joints play an important role in the stability of the whole structure. They are subjected to forces in multiple directions, as shown in Figure 18(a). The baroclinic bar mechanism is shown in Figure 18(b), and the truss mechanism is shown in Figure 18(c).

At the initial stage of loading, when the stirrups could not bear the shear force, the recycled steel fiber-reinforced concrete baroclinic bar formed in the joint core area played a central role. When the shear force at the beam-column joints exceeds the tensile strength of the recycled steel fiber-reinforced concrete, the surface of the joint core area shows the first crack. However, due to the incorporation of recycled steel fiber-reinforced concrete, the tensile strength at the specimen joints is obviously improved, making the initial crack appear later. In the middle of loading, the capacity of the baroclinic bar to bear the baroclinic pressure decreases due to the increase of the displacement and load. At this time, the truss mechanism composed of stirrups, vertical rebars, and recycled steel fiber-reinforced concrete in the joint core area mainly bears the baroclinic tension, and the baroclinic pressure is borne by the baroclinic bar. At the end of loading, the baroclinic pressure is mainly borne by the

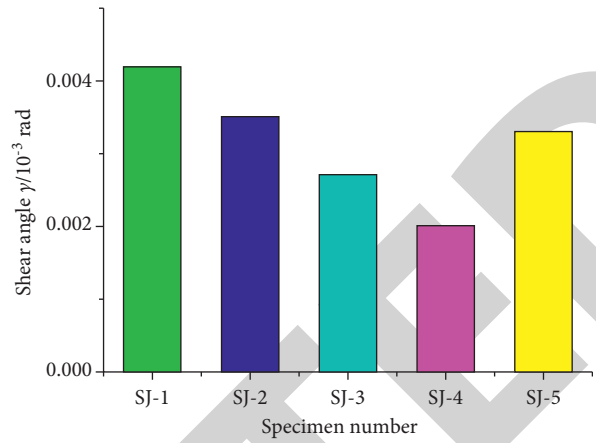

Figure 16: Deformation angles of specimens under the first yield state.

frictional resistance between the cracks at the joints and the bonding force between the recycled steel fiber-reinforced concrete and the rebars.

For ordinary reinforced concrete joint specimens and reinforced concrete joint specimens mixed with normal steel fibers, the anchorage bond between cement mortar, stirrups, longitudinal reinforcements, and recycled steel fibers in recycled steel fiber-reinforced concrete beam-column joints is obviously stronger. The shear force at the joints can be transferred by the bonding force between the rebars and the recycled steel fiber-reinforced concrete so that the shear capacity of the truss mechanism can be better played. Therefore, the action mechanism of the shear capacity of the recycled steel fiber-reinforced concrete frame beam-column joints is the joint action of the barocline bar-truss mechanism.

5.2. Constitutive Relations of Recycled Steel Fibers. Compared with the brittle material (concrete), the constitutive relationship of steel wire recycled from industrial waste tires is not complicated. The nature of recycled steel fibers belongs to steel, and some classical constitutive relations proposed by previous researchers can be adopted and used. So the bilinear follow-up strengthening model is directly adopted in this paper. Therefore, the stress-strain relationship of recycled steel fibers is shown in Figure 19. The initial elastic modulus is E_0, and the plastic modulus (E_1) entering the plastic stage after yielding is 1.0% of the initial elastic modulus, namely,

$$E_1 = 0.01E_0. \tag{7}$$

5.3. Calculation Model of Shear Capacity of Recycled Steel Fiber-Reinforced Concrete Frame Joints. In the calculation of shear capacity of joints, the influence of concrete, column axial pressure, and stirrups at joints is considered in the Chinese code [23], and the design formula is as follows:

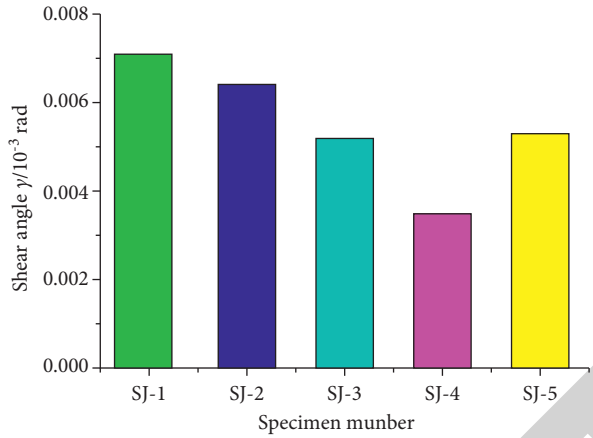

Figure 17: Deformation angles of specimens under the first limit state.

Table 6: Beam end deflection caused by shear deformation in the joint core area.

No.	SJ-1	SJ-2	SJ-3	SJ-4	SJ-5
Beam end deflection under first yield state/mm	6.34	5.29	4.22	3.05	5.01
Beam end deflection under first limit state/mm	10.69	9.65	7.86	5.29	7.99

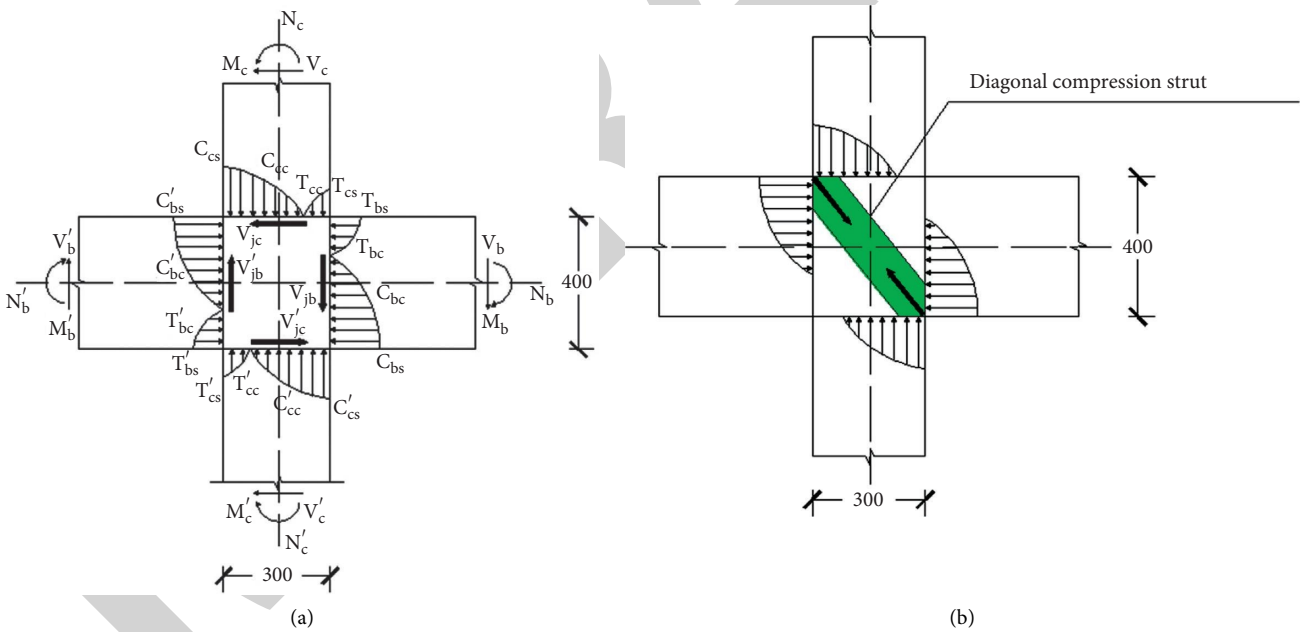

Figure 18: Continued.

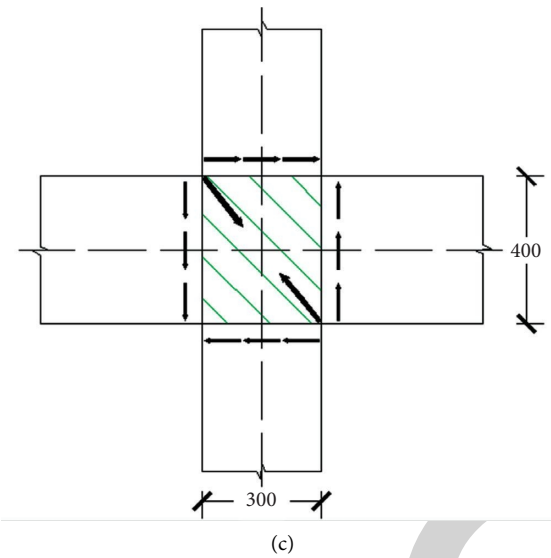

Figure 18: Force diagram of beam-column joints. (a) The force on the joint. (b) Baroclinic bar mechanism. (c) Truss mechanism.

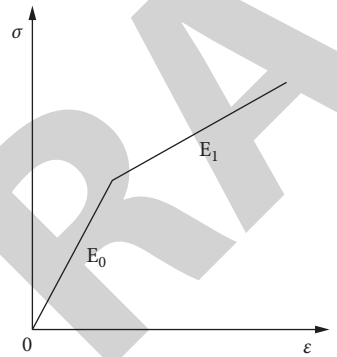

Figure 19: Stress-strain relationship of recycled steel fibers.

$$V_j \leq \frac{1}{\gamma_{RE}}\left[1.1\eta_1 f_t b_j h_j + 0.05\eta_j N\frac{b_j}{b_c} + f_{yv}A_{svj}\frac{h_{bo}-a_s'}{s}\right], \tag{8}$$

where V_j is the shear strength of joints; η_j is the constraint influence coefficients of orthogonal beams on joints; N is the design value of axial force at column end; h_{bo} is the effective height of beam section.

The shear strength design formula of joints specified in the American code is based on the baroclinic bar mechanism, and its design formula is as follows:

$$V_j = 0.083\gamma\sqrt{f_{ck}}b_j h_c, \tag{9}$$

$$b_j = \min\left(\frac{b_j + b_c}{2}, b_b + \sum\frac{mh_c}{2}, b_c\right), \tag{10}$$

where γ is the influence coefficient of joints; f_{ck} is the concrete compressive strength; b_j is the section width of joint core area; m is the coefficient ($m = 0.3$ when the eccentricity of the center of the beam-column joint exceeds $b_c/8$; $m = 0.5$ in other cases).

The stress and shear mechanism of beam-column joint core areas are relatively complex. After referring to the design formula of shear capacity of ordinary reinforced concrete joints, the calculation model of shear capacity of recycled steel fiber-reinforced cruciform concrete frame joints is established, as shown in Figure 20:

$$V_{rj} = V_c + V_s + V_{rf}, \tag{11}$$

where A_{str} is the shear capacity of concrete; θ is the shear capacity of stirrups; V_{rf} is the shear capacity of recycled steel fibers.

(1) Shear capacity V_c of concrete joints. Concrete shear bearing capacity V_c in the baroclinic bar model is determined by the following formula (12):

$$V_c = f_c A_{str}\cos\theta, \tag{12}$$

where A_{str} is the cross-section area of the baroclinic bar; θ is the angle between the baroclinic bar and

bottom longitudinal bar ($\theta = \arctan(h'_b/h'_c)$, h'_b, and h'_c are the spacing of longitudinal bars in the protective layer of beam and column, respectively)

It is found that compressive stress diffusion exists in the process of force transmission of steel fiber-reinforced concrete baroclinic bar [24]. To simplify the calculation, the effective cross-sectional area of the baroclinic bar is determined by the following formula:

$$A_{str} = \frac{kb_s h_c}{\cos\theta}, \tag{13}$$

where k is the comprehensive influence coefficient of effective area of the baroclinic bar; b_s is the cross-section width of the baroclinic bar ($b_s = b_j$, b_j is the joint width); h_c is the height of column end section. For reference, value k is determined by the following formula [25]:

$$k = 0.168(1 + 0.263n)\left(1 + 0.492\lambda_f\right)\left(1 + 6.054\lambda_s\right), \tag{14}$$

where n is the axial compression ratio of column end; λ_f is the characteristic value of steel fiber content ($\lambda_f = \rho_f(l_f/d_f)$); λ_s is the stirrup characteristic value of the joint core area ($\lambda_s = 0.08$).

Softening coefficient λ_{str} ($\lambda_{str} = 0.4$)introduced for barotropic bar mechanism was softened because of cyclic tension and compression [26]. The following formula (15) can be obtained by combining (12) (14):

$$V_c = \lambda_{str} f_c k b_s h_c. \tag{15}$$

(2) Shear capacity of the joint stirrup V_s. In this paper, the shear capacity of the joint stirrups is calculated by using the calculation formula 16 of shear capacity of ordinary reinforced concrete beam-column joint:

$$V_s = f_{yv}\frac{A_{sv}}{S}(h_0 - a'_s), \tag{16}$$

where f_{yv} is the design value of tensile strength; $A_{sv} = nA_{sv1}$, A_{sv} is the total section value of stirrups, n is the total number of stirrups in the same section, and A_{sv1} is the sectional area of the stirrup of a single leg [27]; h_0 is the effective height of joint section; S is the stirrups spacing (the direction is along the beam length and column height); a'_s is the distance between the resultant point of longitudinal reinforcement and the edge of concrete.

According to the experimental analysis, the loss of bearing capacity of joints is due to the existence of the compression area at the beam end and column end, which limits the development of inclined cracks, leading to the stirrups in the joint core area failure to yield completely [28], so the coefficient δ is introduced; assume that the stress within the 2/3 height range in the middle of the joint core area reaches yield, taking $\delta = 2/3$, and obtain the following formula (17):

$$V_{js} = {}_{\delta} f_{yv}\frac{A_{sv}}{S}(h_0 - a'_s). \tag{17}$$

(3) The shear capacity V_{rf} of recycled steel fibers at the joint. There are usually two formulas for calculating the shear capacity of steel fiber-reinforced concrete (SFRC): one is to take SFRC as composite material and use the property that steel fibers can improve the tensile strength of concrete matrix to calculate. The other is to take steel fibers as a separate reinforcement to calculate. Based on the two design formulas of steel fiber-reinforced concrete, the design formulas of shear capacity of recycled steel fibers under different conditions are established, respectively, in this paper:

(1) As composite materials, according to relevant literature [29], the shear capacity of recycled steel fibers is determined by formula (18):

$$V_{rf} = V_{jc}\alpha_f\frac{f_{ft}}{f_t}, \tag{18}$$

where α_f is the influence coefficient of steel fibers on tensile strength of concrete matrix, combining with the test [30], taking $\alpha_f = 0.53$; f_t is the tensile strength of concrete matrix; f_{ft} is the tensile strength of recycled steel fiber-reinforced concrete, and its expression is shown in formula (19).

$$f_{ft} = f_t\left(1 + 1.177\rho_f\left(l_f/d_f\right)\right), \tag{19}$$

where ρ_f is the volume content of steel fibers; l_f/d_f is the length-diameter ratio of steel fibers. Substitute formula (19) into formula (18) to obtain

$$V_{rf} = 0.53V_{jc}\left(1 + 1.177\rho_f\left(l_f/d_f\right)\right). \tag{20}$$

Substitute formulas (15), (17), and (20) into formulas (11) to obtain the design formula (21) for shear capacity of recycled steel fiber-reinforced concrete frame joints:

$$V_{rj} = 0.4f_c k b_s h_c\left[1 + 0.53\left(1 + 1.177\lambda_f\right)\right] + \frac{2}{3}f_{yv}\frac{A_{sv}}{S}(h_0 - a'_s). \tag{21}$$

(2) As an independent reinforcement, considering the bonding stress between steel fibers and concrete mortar when steel fibers are used as independent reinforcement for calculation, the shear bearing capacity of recycled steel fibers can be determined by the following formula:

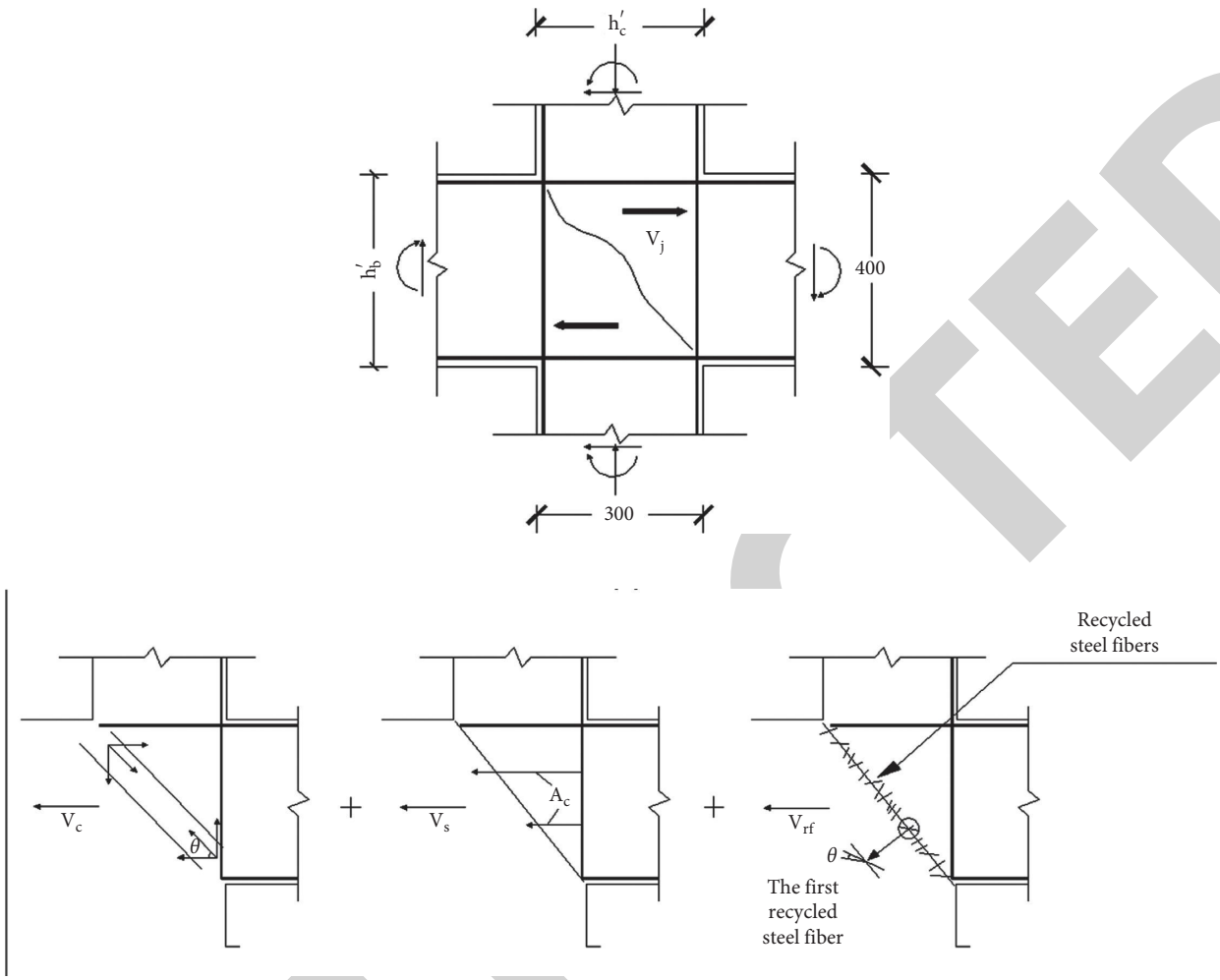

Figure 20: Calculation model of shear capacity of beam-column joints.

$$V_{rf} = \sum_{i=1}^{n_f} \pi \, d\tau_{fi} \cos \theta_i, \tag{22}$$

where n_f is the number of equivalent steel fibers on inclined crack surfaces; τ_{fi} is the bonding stress of the ith steel fiber at inclined crack. The number of steel fibers n_f in the cross crack can be determined by the following formula:

$$n_f = \frac{\alpha_1 \rho_f b_j h_j}{\pi d^2 \sin \theta_1}, \tag{23}$$

where θ_1 is the angle between inclined crack and horizontal axis; α_1 is the nonuniform influence coefficient of recycled steel fibers (approximately taking $\alpha_1 = 0.41$).

Assuming that τ_{fi} and θ_i of each steel fiber at inclined crack are the same, formula (24) can be obtained:

$$V_{rf} = \frac{\alpha_1 \cos \theta_2}{\sin \theta_1} \tau_f \lambda_f b_j h_j, \tag{24}$$

where τ_f is the bonding stress of steel fibers ($\tau_f = \eta_b f_{ft}$, η_b is theinterface bonding coefficient); θ_2 is the angle between steel fibers and horizontal plane.

In the finishing formula (24), taking $\mu = \alpha_1 \eta_b f_{ft} \cos \theta_2 / \sin \theta_1$, the shear capacity V_{rf} of recycled steel fibers is

$$V_{rf} = \mu \eta_b \lambda_f f_{ft} b_j h_j. \tag{25}$$

By inserting formulas (15), (15), and (27) into formulas (11), the calculation model of shear capacity of recycled steel fiber-reinforced concrete can be written:

$$V_{rj} = 0.4 f_c k b_s h_c + \frac{2}{3} f_{yv} \frac{A_{sv}}{S} (h_0 - a_s') + \mu \eta_b \lambda_f \left(1 + 1.177 \lambda_f\right) b_j h_j. \tag{26}$$

Combined with the relevant data in this paper, considering the different bonding effects between recycled steel fibers and concrete, the influence coefficient γ was added,

Table 7: The comparison between the test and calculated results of shear capacity of specimens.

No.	f_{cu}/MPa	f_c'/MPa	Beam size/mm × mm		n	Steel fibers		The stirrups at the joints		v_j^t/MPa	v_j^c/MPa		v_j^t/v_j^c	
			$b_c \times h_c$	$b_b \times h_b$		$\frac{l_f}{d_f}$	ρ_f /%	Number of stirrups	f_y /MPa		Formula (26)	Formula (27)	Formula (26)	Formula (27)
SF-1 [25]	21.3	—	250 × 350	200 × 350	0.32	66	1.20	0	0	325.2	304.2	284.3	1.069	1.144
SF-7 [25]	18.2	—	250 × 350	200 × 350	0.25	54	1.50	3 Φ 6	497	398.6	340.9	361.8	1.169	1.102
A-1 [26]	31.0	—	200 × 250	180 × 300	0.20	80	0.50	0	0	186.4	139.0	123.1	1.341	1.514
A-2 [26]	33.3	—	200 × 250	180 × 300	0.20	80	1.00	0	0	189.5	170.3	172.0	1.113	1.102
SF-1 [27]	21.3	—	250 × 350	200 × 350	0.32	61	1.20	0	0	189.5	298.6	273.7	1.089	1.188
SF-6 [27]	18.2	—	250 × 350	200 × 350	0.25	75	1.50	0	0	330.9	223.9	290.1	1.478	1.141
SF-7 [27]	18.2	—	250 × 350	200 × 350	0.25	75	1.50	3 Φ 6	497	398.6	360.6	426.8	1.105	0.934
SJ-1	30.01	—	300 × 300	250 × 400	0.20	60	0	1 Φ 6	168	200.5	191.6	170.8	1.046	1.174
SJ-2	30.13	—	300 × 300	250 × 400	0.20	60	0.5	1 Φ 6	168	204.6	225.2	190.5	0.909	1.074
SJ-3	31.14	—	300 × 300	250 × 400	0.20	60	1.0	1 Φ 6	168	209.8	244.4	256.1	0.858	0.818
SJ-4	32.35	—	300 × 300	250 × 400	0.20	60	1.5	1 Φ 6	168	213.7	271.6	301.8	0.787	0.708

and the coefficient of recycled steel fiber-reinforced cruciform concrete frame beam-column joints was set as $\gamma = 0.8$, while the coefficient of normal steel fiber-reinforced cruciform concrete frame beam-column joint was set as $\gamma = 0.9$.

In order to verify the rationality of the above design formula, the test data of seven steel fiber-reinforced concrete beam-column joint specimens in the literature [31–33] and the test data of four recycled steel fiber-reinforced concrete cruciform frame joint specimens in this paper are selected as shown in Table 7. According to formulas (21) and (26), the shear capacity of eleven joint specimens is statistically analyzed, and the calculation models of shear capacity of recycled steel fiber-reinforced cruciform concrete frame beam-column joints are fitted, respectively, as follows:

$$V_{rj} = \gamma\left[0.28nf_c b_j h_c\left(1 + 0.53 \times \left(1 + 1.177\lambda_f\right)\right) + \frac{2}{3}f_{yv}\frac{A_{sv}}{s}\left(h_0 - a_s'\right)\right], \tag{27}$$

$$V_{rj} = \gamma\left[0.35nf_c b_j h_c + 0.8\lambda_f\left(1 + 1.177\lambda_f\right)b_j h_j + \frac{2}{3}f_{yv}\frac{A_{sv}}{s}\left(h_0 - a_s'\right)\right]. \tag{28}$$

Table 7 shows the comparison between the shear bearing capacity test values and the calculated values based on formulas (27) and (28). The average value, standard deviation, and variation coefficient of shear capacity of eleven joint specimens are 1.088, 0.191, and 0.176, respectively, in the ratio between the test values and the calculated values of formula (4-27) (27). The average value, standard deviation, and variation coefficient are 1.082, 0.201, and 0.186, respectively, in the ratio between the test values and the calculated values of formula (4-28) (28). The results are in good agreement with each other.

6. Conclusions

In this paper, quasistatic tests were carried out on five cruciform reinforced concrete frame joint specimens to study their seismic performance. By comparing the test results with the formula calculation results, the following main conclusions are drawn:

(1) The addition of normal steel fibers can improve the bearing capacity, ductility, energy dissipation capacity, and shear strength of cruciform concrete frame joint specimens and delay the stiffness degradation of joint specimens, that is, improve the seismic performance of specimens, and the effect of recycled steel fibers is better than normal steel fibers in improving the seismic performance of joint specimens.

(2) With the increase of volume ratio of recycled steel fibers, the seismic performance of joint specimens is improved gradually. Moreover, with the recycled steel fiber content from 0.5% to 1.0% and then to 1.5%, the increased amplitude of the seismic performance of joint specimens increases.

(3) The calculation results of the calculation model of shear capacity of recycled steel fiber-reinforced concrete frame joints are in good agreement with the test results, which can provide references for the calculation of shear capacity of steel fiber-reinforced concrete frame joint specimens.

Data Availability

All the raw data used to support the findings of this study are included within the article. All the raw data are available from the corresponding author upon request.

Conflicts of Interest

The authors declare that they have no conflicts of interest.

Acknowledgments

This work was supported in part by the National Key Research and Development Program of China (no. 2017YFC0806100) and the Jilin Scientific and Technological Planning Project (no. 20210402073GH).

References

[1] L. P. Wang, W. W. Luo, S. W. Liu et al., "Experimental investigation of beam elongation effects on the mechanism and seismic performance of RC frame joints," *Engineering Mechanics*, vol. 37, no. 2, pp. 159–167, 2020.

[2] S. Qudah and M. Maalej, "Application of Engineered Cementitious Composites (ECC) in interior beam-column connections for enhanced seismic resistance," *Engineering Structures*, vol. 69, pp. 235–245, 2014.

[3] A. Aviram, B. Stojadinovic, and G. J. Parra-Montesinos, "High-performance fiber-reinforced concrete bridge columns under bidirectional cyclic loading," *ACI Structural Journal*, vol. 111, no. 2, pp. 303–312, 2014.

[4] G. F. Peng, X. J. Niu, and Q. Q. Long, "Experimental study of strengthening and toughening for recycled steel fiber reinforced ultra-high performance concrete," *Key Engineering Materials*, vol. 629-630, pp. 104–111, 2015.

[5] Z. Z. Kang and B. J. Zhang, "Scrap tires recycling in landscape engineering," *Advanced Materials Research*, vol. 374-377, pp. 1571–1575, 2011.

[6] J. Carrillo, J. Lizarazo-Marriaga, and F. Lamus, "Properties of steel fiber reinforced concrete using either industrial or recycled fibers from waste tires," *Fibers and Polymers*, vol. 21, no. 9, pp. 2055–2067, 2020.

[7] Y. Li, X. P. Wang, G. He Zh et al., "Experimental study on shear behavior of industrial waste fiber reinforced cement matrix composites," *Industrial Construction*, vol. 50, no. 12, pp. 88–92, 2020.

[8] D. Kheni, R. H. Scott, S. K. Deb et al., "Ductility enhancement in beam-column connections using hybrid fiber-reinforced concrete," *ACI Structural Journal*, vol. 112, no. 2, pp. 167–178, 2015.

[9] X.-w. Liang, Y.-j. Wang, Y. Tao, and M.-k. Deng, "Seismic performance of fiber-reinforced concrete interior beam-column joints," *Engineering Structures*, vol. 126, pp. 432–445, 2016.

[10] G. Sh, "Experimental study on seismic behavior of steel fibers locally reinforced high strength concrete frame joints," *Zhengzhou University*, vol. 36, p. 57, 2012 Zhengzhou, Henan Province, China.

[11] M. Ming, S. S. Zheng, H. Zheng et al., "Experimental study on bond slip performance of profile steel high performance fiber-reinforced concrete," *Engineering Mechanics*, vol. 37, no. 8, pp. 148–157, 2020.

[12] E. Eincina, Y. Lu, and R. S. Henry, "Axial elongation in ductile reinforced concrete walls," *Bulletin of the New Zealand Society for Earthquake Engineering*, vol. 49, no. 4, pp. 305–318, 2016.

[13] L. I. Zh, "Study on mechanical properties of steel fiber-reinforced concrete and its application in subway engineering," *Southwest Jiaotong University*, vol. 2018, 2017 Chengdu, Sichuan Province, China.

[14] N. Nourmohammadi, N. P. O'Dowd, and P. M. Weaver, "Effective bending modulus of thin ply fibre composites with uniform fibre spacing," *International Journal of Solids and Structures*, vol. 196-197, pp. 26–40, 2020.

[15] S. G. Liu, R. Bai, C. W. Yan et al., "Experimental study and theoretical calculation of bending stiffness of reinforced fiber reinforced cement matrix composite beams," *Journal of Building Structures*, vol. 39, no. S2, pp. 176–182, 2018.

[16] L. Liao, J. Zhao, F. Zhang, S. Li, and Z. Wang, "Experimental study on compressive properties of SFRC under high strain rate with different fiber content and aspect ratio," *Construction and Building Materials*, vol. 261, p. 119906, 2020.

[17] R. A. Raju, S. Lim, M. Akiyama, and T. Kageyama, "Effects of concrete flow on the distribution and orientation of fibers and flexural behavior of steel fiber-reinforced self-compacting concrete beams," *Construction and Building Materials*, vol. 262, p. 119963, 2020.

[18] Southeast University Tianjin University Tongji University, "Concrete structure," *China Building Industry Press*, China, Beijing, 2020.

[19] Z. H. B. Xu, "Study on seismic behavior of steel fiber-reinforced concrete plastic hinge beam-column joints at beam end," *Tongji University*, China, Shanghai, 2006.

[20] R. Siva Chidambaram and P. Agarwal, "Seismic behavior of hybrid fiber reinforced cementitious composite beam-column joints," *Materials & Design*, vol. 86, pp. 771–781, 2015.

[21] K. F. Gao, "Design and mechanical properties analysis of column-column-beam assembled steel frame joints, Harbin Institute of Technology," *Harbin, Heilongjiang Province, China*, 2018.

[22] H. Zhang, "Early capability and damage analysis of self-compacting, steel-fiber-reinforced lightweight aggregate concrete," *Materials Review*, vol. 31, no. 20, pp. 124–128, 2017.

[23] Code for Concrete Design Structures (GB 50010-2010), *Beijing*, China Building Industry Press, Beijing, China, 2017.

[24] D. Y. Gao, K. Shi, and B. Zhao Sh, "Calculation method of shear capacity of reinforced steel fiber concrete beam-column joints based on softened tension and compression bar model," *Journal of Civil Engineering*, vol. 47, no. 9, pp. 101–109, 2014.

[25] J. W. Zhang, "Study on mechanical properties of steel fiber concrete side joints and legs," *Zhengzhou University*, Zhengzhou, Henan Province, China, 2011.

[26] G. H. Xing, B. Q. Liu, and T. Wu, "Simplified calculation model of shear capacity of reinforced concrete frame joints," *Journal of Building Structures*, vol. 32, no. 10, pp. 130–138, 2011.

[27] L. S. Zhang, "Structural vulnerability evaluation considering elastic-plastic, parameter randomness and internal force contribution of component materials," *Fuzhou University*, Fuzhou, Fujian Province, China, 2018.

[28] Z. Q. Zh and L. Wei, "Wei L Experimental study on shear capacity of steel fiber reinforced concrete frame joints," *Journal of Civil Engineering*, vol. 38, no. 9, pp. 90–93, 2005.
[29] Y. J. An and G. F. Zhao, "Huang Ch K Research on calculation method of bearing capacity of reinforced steel fiber concrete members," *Journal of Civil Engineering*, vol. 26, no. 1, pp. 38–46, 1993.
[30] F. L. Li, B. Zhao Sh, and K. Huang Ch, "Research on shear capacity design method of reinforced steel fiber concrete beams," *Industrial Construction*, vol. 33, no. 10, 4, 2003.
[31] J. R. Tang, C. B. Hu, K. J. Yang et al., "Seismic behavior and shear strength of frames joint using steel-fiber reinforced concrete," *Journal of Structural Engineering, ASCE*, vol. 118, no. 2, pp. 341–358, 1992.
[32] M. J. Shannag, N. Abu-Dyya, and G. Abu-Farsakh, "Lateral load response of high performance fiber reinforced concrete beam-column joints," *Construction and Building Materials*, vol. 19, no. 7, pp. 500–508, 2005.
[33] Y. Li, X. L. Wang, and Q. J. Ding, "Effect of length and content of steel fiber on mechanical properties of concrete," *Concrete*, no. 7, pp. 62–65, 2017.